

Adjoint diagnostics for the atmosphere and ocean

Jan Barkmeijer

*Royal Netherlands Meteorological Institute
de Bilt, The Netherlands
Jan.Barkmeijer@knmi.nl*

ABSTRACT

Adjoint models have found their way to many applications in numerical weather prediction, such as variational data assimilation, singular vector analysis and sensitivity studies. This paper lists some examples of how adjoint models are being used as a diagnostic tool in atmospheric and ocean models. Their variety is indicative for the many opportunities adjoint models provide in helping to understand the behaviour of these models.

1 Introduction

The use of adjoint models as a diagnostic tool has increased rapidly over the last years in the atmospheric and ocean community. This is not surprising given the capability of adjoint models to inform efficiently about various aspects of model behaviour. An important area of such an adjoint application is provided by the data-assimilation scheme. In particular the way observations exert impact on the forecast performance is one of the issues that can be addressed. For more details about this diagnostic application of adjoint models we refer to the paper by Cardinali (these Proceedings). Other areas where adjoint models play a diagnostic role are associated with sensitivity and stability issues. With respect to sensitivity, one is interested in how much an aspect of the model behaviour, e.g. the 2-day forecast error, will change when perturbations are allowed in the forecast production process. This, for example, may concern parameter variations in parametrized physical processes or perturbations to the model initial condition. In case of models with many degrees of freedom the model's adjoint provides an efficient way to inform about such sensitivity related questions, see e.g. Rabier *et al.* (1992, 1996); Errico and Vukićević (1992). In case of stability issues one would like to know, for example, how large forecast deviations one may expect when reasonable perturbations are allowed to the model environment, such as the initial condition or physical parametrization scheme. Also here adjoint models proved to be useful in, for example, assessing the dominant growing structures present in the initial condition of a model (Lorenz, 1969). The further study of these so-called non-modal structures, e.g. Farrell and Ioannou 1996a,b, has been very fruitful, particularly in the progress of predictability research.

In this paper we present some examples of how adjoint models can be used as diagnostic tool. We certainly do not claim that this overview is complete. It hopefully does illustrate that there are many opportunities to explore the use of adjoint models, see also Errico (1997) in this context. However, there are also limitations to the applicability of adjoint models, which are inherently associated with linear models. To overcome the restriction of linear perturbation growth there have been attempts to extend the concept of adjoint models to the weakly nonlinear regime, e.g. Oortwijn and Barkmeijer (1995) and Mu *et al.* (2003). Another issue which we do not touch in this paper is the growing complexity of nonlinear forecast models. For an overview of the problems this poses for the derivation of the tangent linear and adjoint model, we refer to Janisková (2003).

The paper is organized as follows. In section 2 we introduce the adjoint model by means of the gradient

computation, which is central to sensitivity calculations. This is followed by a series of applications in section 3, where adjoint models are being used as diagnostic tools.

2 Tangent and adjoint model

In this section we show how an adjoint model can be used to efficiently determine the gradient of a function. This property is essential in many applications, for example in minimizing the costfunction in variational data-assimilation.

Suppose we are dealing with a nonlinear model M , which for a given input \mathbf{x} produces the output \mathbf{y} after some time integration:

$$d\mathbf{x}/dt = M(\mathbf{x}) \quad (1)$$

and further with a differentiable function J , which is defined for the model output field \mathbf{y} :

$$J = J(\mathbf{y}) = J(M(\mathbf{x})) \quad (2)$$

The function J may be a simple function of the output \mathbf{y} , but the computation of its gradient with respect to \mathbf{x} is another matter:

$$\frac{\partial J}{\partial x_j} = \sum_k \frac{\partial J}{\partial y_k} \frac{\partial y_k}{\partial x_j} \quad (3)$$

The gradient of J would require a perturbed run for every entry of \mathbf{x} (which is $O(10^8)$ in case of operational NWP models). Assume that perturbations evolve linearly and that a small perturbation δy_j of y_j is associated to a perturbation δx_k of x_k through:

$$\delta y_j = \sum_k \frac{\partial y_j}{\partial x_k} \delta x_k =_{def} (\mathbf{M}\delta\mathbf{x})_j \quad (4)$$

Then we can write

$$\nabla_{\mathbf{x}} J = \mathbf{M}^T \nabla_{\mathbf{y}} J \quad (5)$$

So provided there is a way to determine the transpose of the operator \mathbf{M} , the gradient $\nabla_{\mathbf{x}} J$ of J can be evaluated. In fact there is and it is the adjoint model which makes this possible:

Suppose that the time evolution of initial condition perturbations for system given by eq. 1 is linear and given by the tangent linear system

$$d\boldsymbol{\varepsilon}/dt = \mathbf{L}\boldsymbol{\varepsilon} \quad (6)$$

with propagator \mathbf{M} : $\boldsymbol{\varepsilon}(t_2) = \mathbf{M}(t_1, t_2)\boldsymbol{\varepsilon}(t_1)$. Define the adjoint model by

$$d\boldsymbol{\varepsilon}/dt = -\mathbf{L}^* \boldsymbol{\varepsilon} \quad (7)$$

where \mathbf{L}^* is the unique operator such that $\langle \mathbf{L}\mathbf{a}, \mathbf{b} \rangle = \langle \mathbf{a}, \mathbf{L}^*\mathbf{b} \rangle$ and $\langle \cdot, \cdot \rangle$ is a suitable innerproduct. Note that $\mathbf{L}^* = \mathbf{L}^T$ in case of the Euclidean innerproduct $[\mathbf{a}, \mathbf{b}] = \sum a_i b_i$. Denote by \mathbf{S} the propagator of the adjoint model. Solutions $\mathbf{a}(t)$ and $\mathbf{b}(t)$ of eqs. 6 and 7 respectively satisfy:

$$d/dt \langle \mathbf{a}(t), \mathbf{b}(t) \rangle = \langle \mathbf{L}\mathbf{a}(t), \mathbf{b}(t) \rangle + \langle \mathbf{a}(t), -\mathbf{L}^*\mathbf{b}(t) \rangle = 0 \quad (8)$$

and consequently

$$\langle \mathbf{M}(t_1, t_2)\mathbf{a}(t_1), \mathbf{b}(t_2) \rangle = \langle \mathbf{a}(t_1), \mathbf{S}(t_2, t_1)\mathbf{b}(t_2) \rangle \quad (9)$$

We conclude that $\mathbf{M}^*\mathbf{y}$ for a given \mathbf{y} can be evaluated by integrating the adjoint model eq. 7 backwards in time starting with initial condition \mathbf{y} .

3 Examples of adjoint models as diagnostic tool

Some examples are presented of how adjoint models are being used in the atmospheric and ocean community. Although the list is far from complete, its diversity reflects the opportunities adjoint models provide in gaining knowledge of atmospheric and ocean processes. It is worth mentioning here that since 1992 a workshop (see Errico and Ehrendorfer (2007) for a review of the seventh workshop (1997) and Adjoint Workshop (1997) for topics presented there) is being held every two years entirely focusing on adjoint model applications.

3.1 Periodic Weather

In a well known application of adjoint models, a perturbation of the initial condition is sought such that the forecast started from the modified initial condition improves. This so-called sensitivity calculation (Rabier 1996; Klinker *et al.* 1998) is a powerful tool in assessing the relative impact of model variables. However, care should be taken with its interpretation (Isaksen *et al.*, 2005; Caron *et al.*, 2007). A minor adaptation of the sensitivity calculation enables the search for Unstable Periodic Orbits (UPO) in model or observational data. UPOs can be considered as the "skeleton" of a dynamical system as given by eq. 1 and knowledge of them (and typically from only a few UPO's with short period) can already inform about the underlying dynamics (Grebogi *et al.*, 1998; Hunt *et al.*, 1996). There is observational evidence that the atmosphere may exhibit UPO's. In Branstator (1987) and Kushnir (1987), for example, a westward-propagating wave is identified in Northern Hemisphere winter analyses of the 500-hPa height with a period of around 23 days. In order to determine UPO's, it suffices to adapt the usual costfunction of the sensitivity calculation. Let $\mathbf{x}(t)$ be a solution of eq. 1. In stead of measuring the difference between the forecast field $\mathbf{x}(T)$ with the verifying analysis for a certain lead time T , the costfunction J is given by:

$$J(\mathbf{x}(0)) = 1/2 \|\mathbf{x}(0) - \mathbf{x}(T)\|^2 \text{ with } \|\cdot\| \text{ some suitable norm} \quad (10)$$

The gradient of J , which is required in the minimization, is then

$$\nabla J = [\mathbf{M}^* - \mathbf{Id}](\mathbf{x}(T) - \mathbf{x}(0)) \quad (11)$$

where \mathbf{M}^* the propagator of the adjoint model with respect to the innerproduct associated with the $\|\cdot\|$ norm and \mathbf{Id} the identity operator. In figure 1 the result of such a minimization is presented. The minimization is performed in the context of a three level quasi-geostrophic model (Marshall and Molteni, 1993). Only a small change to the original $\mathbf{x}(0)$ results in a loop in phase space with a period of 10 days.

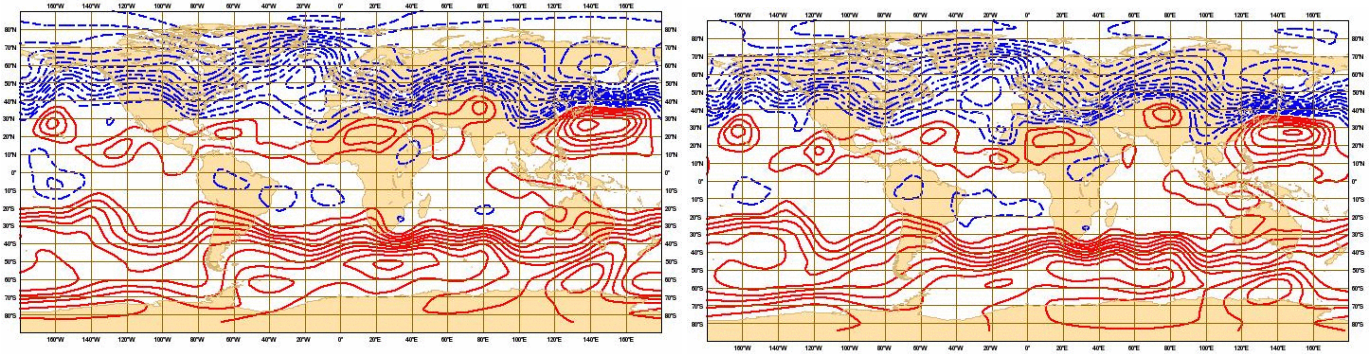


Figure 1: Original initial condition $\mathbf{x}(0)$ (left) and after minimization (right) in terms of streamfunction at 500 hPa. Positive and negative values are plotted in red and blue respectively, with contour interval $3.0 \times 10^6 \text{m}^2 \text{s}^{-1}$. The modified initial condition produces a UPO with a period of 10 days.

3.2 Upwelling cells

In a sensitivity type of experiment (Chhak and Di Lorenzo, 2007) the origin of coastally upwelled water off the coast of California is determined using the ocean model ROMS (Haidvogel *et al.*, 2000) and its adjoint ADROMS (Moore *et al.*, 2004). It appears that in the "cool" phase (pre mid-1970s) of the Pacific Decadal Oscillation (PDO), the upwelling cell is deeper while during the "warm" phase (post mid-1970s), the upwelling cell is shallower with more horizontal entrainment of surface waters from the north, see Fig 2. This reduction of nutrient rich deep waters being vertically mixed to the surface may play a role in the observed decline in zooplankton biomass off the coast of California after the mid 1970s.

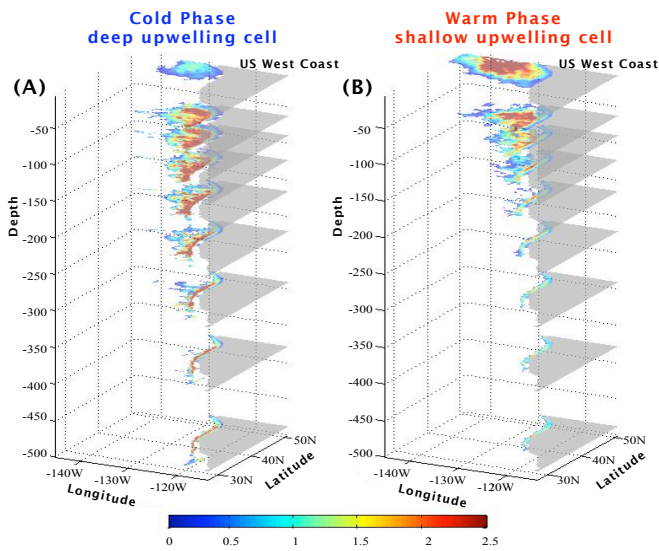


Figure 2: Percent ratio of the origin of coastally upwelled waters one year prior to peak upwelling indicating the origin of coastally upwelled water for the (A) cold and (B) warm phase of the Pacific Decadal Oscillation. From Chhak and Di Lorenzo (2007).

3.3 Sensitivity in two convection schemes

Central in the study of Mahfouf and Bilodeau (2007) is to evaluate the sensitivity of surface precipitation to the initial condition for up to 24 h. They perform their experiments with the Global Environmental Multi-scale (GEM) model, together with the tangent linear and adjoint version of its dynamical core (Tanguay and Polavarapu, 1999) and of a simplified physics package (Zadra *et al.*, 2004). In particular the impact of the definition of the moist convection scheme's closure on the adjoint sensitivities is studied. The formulation of deep convection is based on a Kuo symmetric scheme (Mahfouf, 2005). Simplifications to the linearized versions lead to two different expressions of the perturbed surface convective rainrate R'_c :

$$R'_{c1} = \int_{pb}^{pt} \left(\frac{\partial q'}{\partial t} \right)_{LS} \frac{dp}{g} \quad \text{and} \quad R'_{c2} = -\frac{C_p}{L} \int_{pb}^{pt} \left(\frac{\partial T'}{\partial t} \right)_{LS} \frac{dp}{g} \quad (12)$$

The subscript LS stands for "large scale" and corresponds to the dynamical tendencies plus tendencies from the dry physics. Mahfouf (2005) has shown that R'_{c1} and R'_{c2} have comparable mean and extreme values, and also the same accuracy with respect to the nonlinear reference. Figure 3 shows the sensitivity of the linearized convection scheme using R'_{c1} (q -closure formulation), and the scheme using R'_{c2} (T -closure formulation in case of a midlatitude case). The diagnostic function J for which the sensitivity is shown is the mean precipitation rate produced by the model at certain lead time T over a geographical domain. Observe that the time axis denotes the integration time of the adjoint model. So $T = 0$ refers to the beginning of the adjoint integration, while $T = 24$ denotes the end of the integration at analysis time. Clearly the closure of the convection scheme has significant impact on the sensitivity of the various components of the model state vector shown, especially in the 0-12h window. With respect to analyses obtained with 4D-VAR it is likely that they are sensitive to the convection closure's scheme or when observations are assimilated close to the beginning of the window.

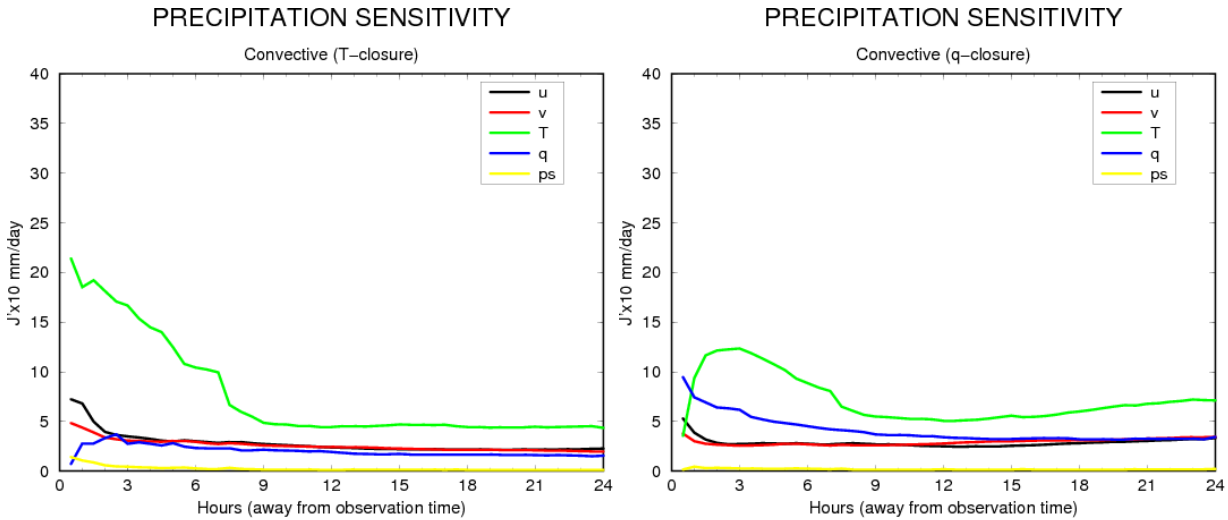


Figure 3: Changes of the diagnostic function J due to optimal perturbation of u , v , T , q , and p_s for instantaneous precipitation at time $t=0$ and for a convection scheme with (left) T -closure and (right) q -closure. From Mahfouf and Bilodeau (2007).

3.4 Singular vectors

Without doubt the sustained interest in singular vectors has been instrumental in various aspects of predictability research. For instance their property to sample the growing component of the initial condition was very appealing to employ in ensemble forecasting (Molteni and Palmer, 1993; Buizza and Palmer, 1995). The adjoint model again enabled an efficient computation of these structures:

$$\frac{\langle \mathbf{E}\mathbf{M}\boldsymbol{\varepsilon}(0), \boldsymbol{\varepsilon}(0) \mathbf{M}\boldsymbol{\varepsilon}(0) \rangle}{\langle \mathbf{C}\boldsymbol{\varepsilon}(0), \boldsymbol{\varepsilon}(0) \rangle} = \frac{\langle \mathbf{M}^*\mathbf{E}\mathbf{M}\boldsymbol{\varepsilon}(0), \boldsymbol{\varepsilon}(0) \rangle}{\langle \mathbf{C}\boldsymbol{\varepsilon}(0), \boldsymbol{\varepsilon}(0) \rangle} \quad (13)$$

where the operators \mathbf{C} and \mathbf{E} induce perturbations norm at initial and optimization time respectively. For sufficiently simple operators \mathbf{C} , maximizing the ratio in eq. 13 corresponds to solving an eigenvalue problem involving the propagators of the tangent linear and adjoint model. In this way one may even find growing structures when the underlying dynamics is stable (Farrell, 1988). A popular choice is identical \mathbf{C} and \mathbf{E} , both inducing the total energy norm. But also more exotic choices are possible, such as a precipitation measuring norm (Errico and Fillion, 2003) or the intensity of the Meridional Overturning Circulation (see section 3.4). In order to constrain the SVs by the best available estimate of analysis error covariance matrix \mathbf{A} one would like to use for \mathbf{C} the Hessian of the 4D-Var costfunction J_{4dvar} . Under mild conditions the following identity holds:

$$\nabla\nabla J_{4dvar} = \mathbf{B}^{-1} + \mathbf{H}^T\mathbf{R}^{-1}\mathbf{H} = \mathbf{A}^{-1} \quad (14)$$

where \mathbf{B} and \mathbf{R} denote the background and observational error covariance matrix respectively and \mathbf{H} is the linearization of the observation operator. Equivalent to eq. 13 these so-called Hessian singular vectors (HSV) also satisfy

$$\mathbf{M}^*\mathbf{E}\mathbf{M}\boldsymbol{\varepsilon}(0) = \lambda\mathbf{A}^{-1}\boldsymbol{\varepsilon}(0) \quad (15)$$

From this we conclude that the weighted time evolved HSVs given by $\mathbf{E}^{1/2}\mathbf{M}\boldsymbol{\varepsilon}(0)$ are the dominant eigenvectors of the forecast error covariance matrix in E-norm: $\mathbf{E}^{1/2}(\mathbf{M}\mathbf{A}\mathbf{M}^*)\mathbf{E}^{1/2}$. For pre-multiplying eq. 15 on both sides with $\mathbf{E}^{1/2}\mathbf{M}\mathbf{A}$ yields:

$$(\mathbf{E}^{1/2}\mathbf{M}\mathbf{A})\mathbf{M}^*\mathbf{E}\mathbf{M}\boldsymbol{\varepsilon}(0) = \lambda(\mathbf{E}^{1/2}\mathbf{M}\mathbf{A})\mathbf{A}^{-1}\boldsymbol{\varepsilon}(0) \quad (16)$$

or

$$(\mathbf{E}^{1/2}\mathbf{M}\mathbf{A}\mathbf{M}^*\mathbf{E}^{1/2})\mathbf{E}^{1/2}\mathbf{M}\boldsymbol{\varepsilon}(0) = \lambda\mathbf{E}^{1/2}\mathbf{M}\boldsymbol{\varepsilon}(0) \quad (17)$$

Recent experimentation at ECMWF (Lawrence *et al.*, 2009) showed that the wavenumber spectra of the initial and final time HSVs now resemble more the spectra of the regular total energy SVs than they used to do (Barkmeijer *et al.*, 1999). Most likely this can be attributed to the revised description of the background error statistics (Fisher, 2003). Contrary to total energy SVs, kinetic energy still dominates potential energy for initial HSVs, see Fig. 4. This property has not changed, see also Palmer *et al.* (1998), Gelaro *et al.* (2002) and Reynolds *et al.* (2006).

3.5 Sea Surface Salinity SVs

In Sévellec *et al.* (2008) singular vectors are computed in order to modify the intensity of the Meridional Overturning Circulation (MOC) at 48°N. At initial time only amplitude in the sea surface salinity (SSS) component of the model state vector is present. The SV amplification depends on the optimization time T , the forecast time during which perturbation growth is maximized. For values ranging from 0.5 to 35 yr, maximum amplification is achieved for $T = 10.5$ yr (see Fig. 5, top right). The corresponding leading SV for $T = 10.5$ yr is shown in Fig. 5 (left). Its location is in the north of the basin, well away from the target region. The linear

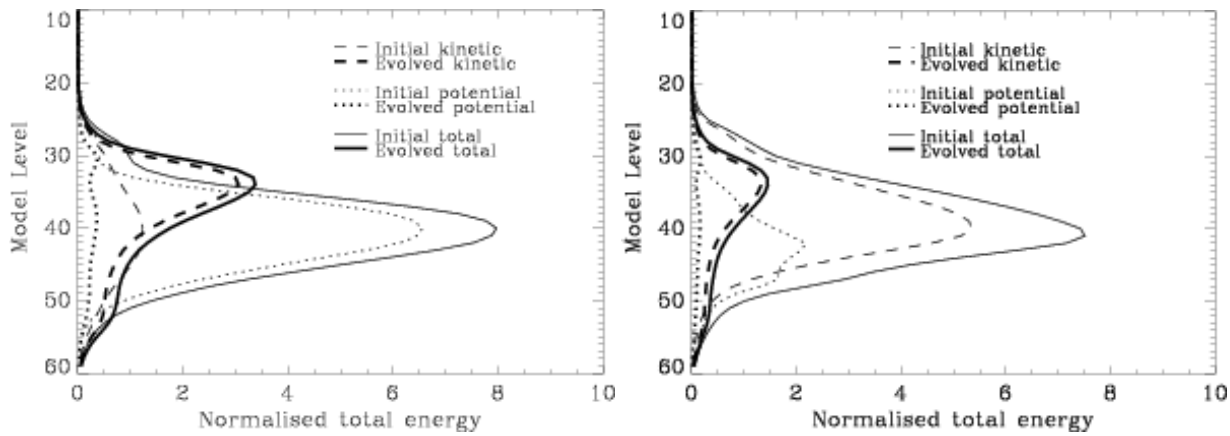


Figure 4: Average vertical energy profiles (over the leading 12 SVs) for (left) TESVs and (right) full HSVs. Values at initial time (thin lines) have been scaled by a factor of 100. From Lawrence et al. (2009).

evolution with unit initial norm is presented in Fig. 5 (right) showing a maximum impact on the MOC intensity at $T = 10.5$ yr. Comparison with nonlinear model integrations indicate that the linear approximation holds well for realistic SSS perturbations. Using typical amplitudes of the Great Salinity Amplitude (Belkin *et al.*, 1998) an upper bound of the MOC intensity variability is obtained of 0.8 Sv ($1 \text{ Sv} = 10^6 \text{ m}^3 \text{ s}^{-1}$), which is 10.5% of the mean circulation. Also SVs were considered solely with amplitude in the sea surface temperature at initial time. These structures, although quite similar to the one of SSS, appeared to be less effective

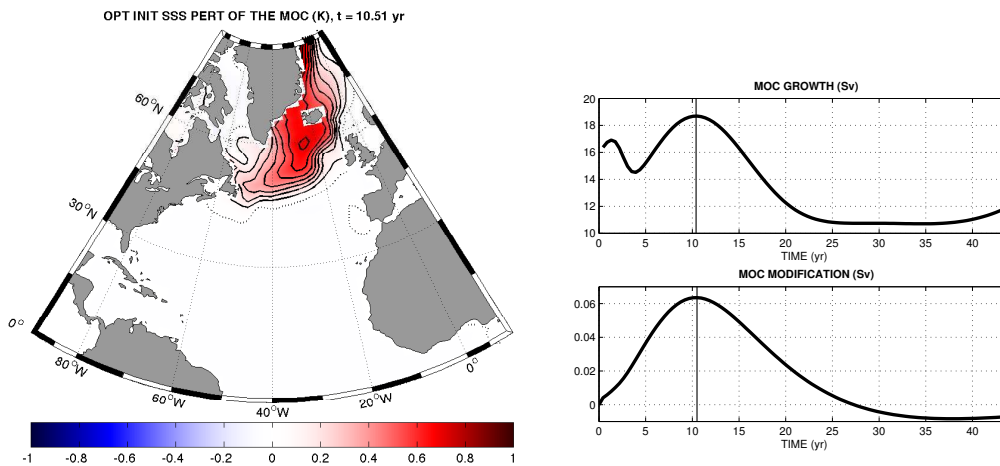


Figure 5: (left) Sea Surface Salinity (SSS) perturbation, which most efficiently modifies the intensity of the Atlantic Meridional Overturning Circulation (MOC) after 10.5 yr. The contour interval is 0.1 psu. (top right) Growth of the MOC as a function of the optimization time, and (top left) MOC intensity during the time integration of the linear model initialized by the SSS perturbation shown in Fig 5 (left). From Sévellec et al. (2008)

3.6 Forcing

In stead of diagnosing the role of the initial condition perturbations by means of adjoint models, the same approach can be applied to studying the impact of model tendency perturbations on, for example, forecast performance. This means that an additional error source term is added to the linear model eq. 6:

$$d\boldsymbol{\varepsilon}/dt = \mathbf{L}\boldsymbol{\varepsilon} + \mathbf{f}(t) \quad (18)$$

where $\mathbf{f}(t)$ is a model tendency perturbation, which is allowed to vary in time. Solutions of eq. 18, which now describes the combined evolution of initial and tendency perturbations, are given by:

$$\boldsymbol{\varepsilon}(t) = \mathbf{M}\boldsymbol{\varepsilon}(0) + \int_0^t \mathbf{f}(s)ds \quad (19)$$

$$= \mathbf{M}\boldsymbol{\varepsilon}(0) + \mathcal{M}\mathbf{f} \quad (20)$$

Just like regular SVs so-called forcing singular vectors (FSVs) can be computed (Barkmeijer *et al.*, 2003) by searching for unit forcings \mathbf{f} that result in maximal response $\langle \mathcal{M}\mathbf{f}, \mathcal{M}\mathbf{f} \rangle = \langle \mathcal{M}^* \mathcal{M}\mathbf{f}, \mathbf{f} \rangle$ at optimization time for a suitable innerproduct $\langle \cdot, \cdot \rangle$. The Reynolds system (see also Farrell and Ioannou, 2005) provides an easy example to compute FSVs. It also nicely illustrates that short-term amplification is possible even in stable systems. The Reynolds system is defined by choosing

$$\mathbf{L} = \begin{pmatrix} -1 & 10 \\ 0 & -2 \end{pmatrix}$$

The left panel of Fig. 6 shows both components of the leading FSV with an optimization time of 4 units and the right panel gives the norm of the perturbation at optimization time for the leading regular SV and FSV. Note that from a certain optimization time onward it is not possible anymore to find growing initial condition perturbations.

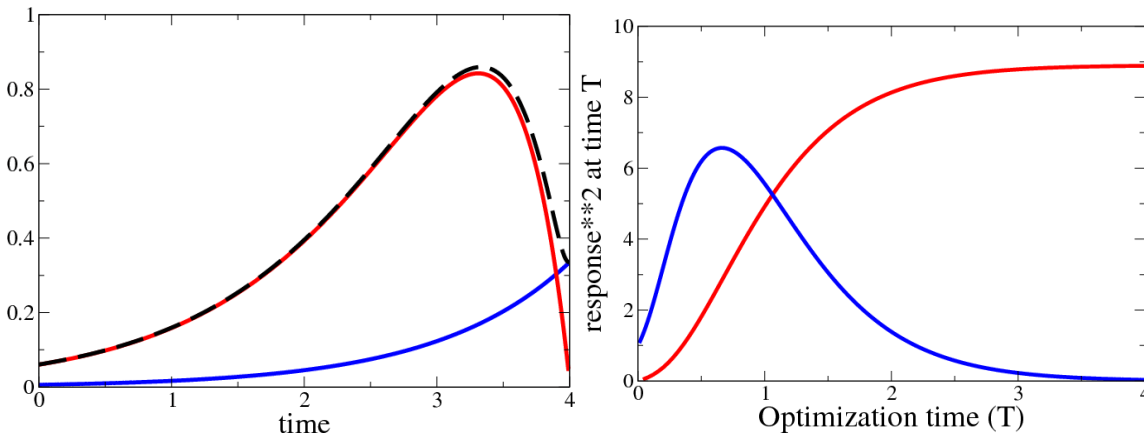


Figure 6: (left) Both components (red and blue line) of the leading time varying FSV of the Reynolds system, together with the norm (dashed line); (right) Norm of the response for the leading SV (blue line) and leading FSV (red line) as a function of optimization time.

When applied in the sensitivity calculation at ECMWF, the tendency perturbations \mathbf{f} were quite capable to improve 10 day forecasts, see Fig 7. In determining the forcing \mathbf{f} the same set-up was used as for the regular sensitivity calculation at ECMWF, such as the number of iterations employed in the minimization of the cost-function. The only difference with the default sensitivity calculation is that the costfunction, given by the total

energy of the 2-day forecast error, can only decrease by searching for a suitable tendency perturbation. To simplify the computation the forcing was kept constant during the optimization time of 2 days. More details can be found in Barkmeijer *et al.* (2003). Recently (Iversen *et al.*, 2008) the forcing approach in the sensitivity calculation has also been used to determine the climate sensitivity with respect to the so-called 'cold-ocean-warm-land' flow regime.

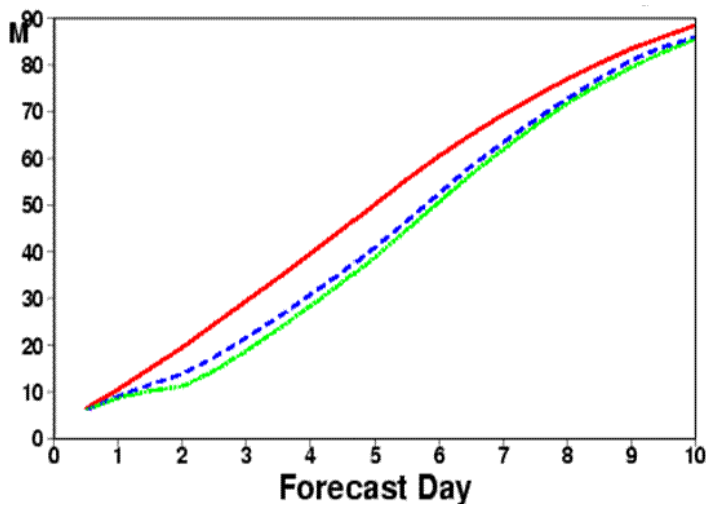


Figure 7: Average T_{L159} forecast performance (39 cases) for northern hemisphere geopotential height in terms of RMS error at 500 hPa. The lines represent unperturbed forecasts (red), with analysis perturbations (blue) and with tendency perturbations (green).

3.7 Increasing the Atlantic subtropical jet

The triggers for abrupt climate changes have generally been thought of as residing in the coupled land-ice/ocean system. For example, massive outflows of glacial meltwater would dilute the waters of the northern North Atlantic to the point that deep convection, essential for maintaining the Meridional Overturning Circulation (MOC), would be halted. This would reduce the oceanic heat transport drastically, resulting in a much cooler climate for the circum-Atlantic region. Recently this hypothesis has been challenged (Broecker, 2006). An alternative hypothesis on the trigger of rapid climate change involves a more active role for the atmosphere. In this view, the Atlantic eddy-driven jet shifts from a southeast-northwest orientation to a zonally oriented position near the subtropical jet. Consequently, the atmospheric meridional heat transport into mid- and high-latitudes is drastically reduced. In a recent study (Lee and Kim, 2003) the repositioning of the eddy-driven jet can be achieved by strengthening the subtropical jet. Van der Schrier *et al.* employ ECBilt-Clio, a coupled ocean atmosphere-sea ice general circulation model of intermediate complexity (Opsteegh *et al.* 1998, Goose and Fichet, 1999) to determine tendency perturbations \mathbf{f} (see section 3.6) which are designed to strengthen the subtropical jet over the North Atlantic sector. More precisely, the linear response $\mathcal{M}\mathbf{f}$ of \mathbf{f} will project maximally on a target pattern, which is associated with a strong subtropical jet. During the coupled model run such forcings \mathbf{f} are computed every 72 h and using an optimization time of 72 h. After the computation of the forcing, the coupled model is continued applying the constant tendency perturbation \mathbf{f} during the model integration. This forcing is then updated again in the next 72 h. During 10-year simulations the model atmosphere is thus forced to a desired pattern, while at the same time synoptic-scale variability internal to the atmospheric or climatic system is not suppressed and can adjust to the changes in the large-scale atmospheric circulation. Fig. 8 shows the change in 2 m DJF- temperature with respect to the control climate, showing an overall cooling

with a decrease in temperature reaching up to 5°C in Western-Europe.

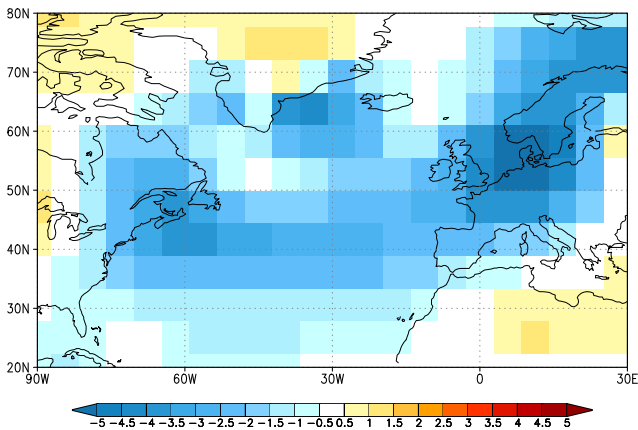


Figure 8: Change in surface air temperature ($^{\circ}\text{C}$) for winter (DJF) in the tendency perturbed simulation compared to the control simulation. From Van der Schrier et al. (2007).

4 Acknowledgements

I would like to thank B. Bolideau, E. Di Lorenzo, A.R. Lawrence, M. Leutbecher, A. Moore, G. van der Schrier and F. Sévellec for providing contributions to this seminar paper.

5 references

Adjoint Workshop, 2007: Special issue: Adjoint Applications in dynamic meteorology (R.N. Errico and M. Ehrendorfer, Eds), *Meteorol. Z.*, **16**, 227p.

Barkmeijer, J., R. Buizza, and T.N. Palmer, 1999: 3D-Var Hessian singular vectors and their potential use. *Q.J.R. Meteorol. Soc.*, **124**, 1695-1713.

Barkmeijer, J., T. Iversen, and T.N. Palmer, 2003: Forcing singular vectors and other sensitive model structures. *Q.J.R. Meteorol. Soc.*, **129**, 2401-2423

Belkin, I.M., S. Levitus, J. Antonov, and S.-A. Malmberg, 1998: "Great salinity anomalies" in the North Atlantic. *Prog. Oceanogr.*, **41**, 1-68.

Broecker, W.S., 2006: Was the Younger Dryas triggered by a flood? *Science*, **312**, 1146-1148.

Buizza, R., and T.N. Palmer, 1995: The singular-vector structure of the atmospheric global circulation. *J. Atmos. Sci.*, **52**, 1434-1456.

Chhak, K., and E. Di Lorenzo, 2007: Decadal variations in the California Current upwelling cells. *Geophys. Res. Lett.*, **34**, L14604, doi:10.1029/2007GL030203

Caron, J.-R., M.K. Tua, S. Laroche, and P. Zwack, 2007: The characteristics of key analysis errors. Part I: Dynamical balance and comparison with observations. *Mon. Wea. Rev.*, **135**, 249-266.

Errico, R.M., and T. Vukićević, 1992: Sensitivity analysis using an adjoint of the PSU-NCAR mesoscale model. *Mon. Wea. Rev.*, **120**, 1644-1660.

Errico, R.M., 1997: What is an adjoint model? *Bull. Amer. Meteor. Soc.*, **78**, 2577-2591.

Errico, R.N., and L. Fillion, 2003: Examination of the accuracy of precipitation rates to possible perturbations of the initial conditions. *Tellus*, **55A**, 88-105.

Errico, R.M., and M. Ehrendorfer, 2007: Adjoint model applications in dynamic meteorology. *Bul. Am. Meteorol. Soc.*, **88**, 1979-1981.

Farrell, B.F., 1988: Optimal excitation of neutral Rossby waves. *J. Atmos. Sci.*, **45**, 163-172.

Farrell, B.F., and P.J. Ioannou, 1996a: Generalized stability theory. Part I: Autonomous operators. *J. Atmos. Sci.*, **53**, 2025-2040.

Farrell, B.F., and P.J. Ioannou, 1996b: Generalized stability theory. Part II: Nonautonomous operators. *J. Atmos. Sci.*, **53**, 2041-2053.

Farrell, B.F., and P.J. Ioannou, 2005: Distributed forcing of forecast and assimilation error systems. *J. Atmos. Sci.*, **62**, 460-475.

Fisher, M., 2003: Background error covariance modelling. In *Proceedings of the ECMWF Workshop on Recent Developments in Data Assimilation for Atmosphere and Ocean*, 8-12 September 2003, Reading UK, pp 45-64.

Gelaro, R., T. Rosmond, and R. Daley, 2002: Singular vector calculations with an analysis error variance metric. *Mon. Wea. Rev.*, **130**, 1166-1186.

Goosse, H., and T. Fichefet, 1999: Importance of sea-ocean interactions for the global ocean circulation: a model study. *J. Geophys. Res. (Oceans)*, **104**, 23337-23355.

Grebogi C., E. Ott and J.A. Yorke, 1988: Unstable Periodic Orbits and the Dimensions of Multifractal Chaotic

Attractors. *Phys. Rev. A*, **37**,: 1711.

Haidvogel, D.B., H.G. Arango, K. Hedstrom, A. Beckmann, P. Malanotte-Rizzoli, and A.F. Shchepetkin, 2000: Model evaluation experiments in the North Atlantic basin: simulations in nonlinear terrain-following coordinates. *Dyn. Atmos. Ocean*, **32**, 239-281.

B Hunt and E Ott (1996) Optimal Periodic Orbits of Chaotic Systems. *Phys. Rev. Letts.* 76: 2254.

Isaksen, L., M. Fisher, E. Andersson, and J. Barkmeijer, 2005: The structure and realism of sensitivity perturbations and their interpretation as 'key analysis errors'. *Q.J.R. Meteorol. Soc.*, **131**, 3053-3078.

Iversen, T., J. Kristiansen, T. Jung, and J. Barkmeijer, 2008: Optimal atmospheric forcing perturbations for the cold-ocean warm-land pattern. *Tellus*, **60 A**, 528-546.

Janisková, M., 2003: Physical processes in adjoint models: potential pitfalls and benefits. In *Proceedings of the ECMWF Seminar on Recent Developments in Data Assimilation for Atmosphere and Ocean*, 8-12 September 2003, Reading, UK, pp 179-291.

Klinker, E., F. Rabier, and R. Gelaro, 1998: Estimation of key analysis errors using the adjoint technique. *Q.J.R. Meteorol. Soc.*, **124**, 1909-1933.

Lawrence, A.R., M. Leutbecher, and T.N. Palmer, 2009: The characteristics of Hessian singular vectors using an advanced data assimilation scheme. *Q.J.R. Meteorol. Soc.*, **135**, 1117-1132.

Lee, S., and H.-K. Kim, 2003: The dynamical relationship between subtropical and eddy-driven jets. *J. Atmos. Sci.*, **60**, 1490-1503.

Lorenz, E.N., 1969: The predictability of a flow which possesses many scales of motions. *Tellus*, **21**, 289-307.

Mahfouf, J.-F., 2005: Linearization of a simple moist convection scheme for large-scale NWP models. *Mon. Wea. Rev.*, **133**, 1655-1670.

Mahfouf, J.-F., and B. Bolideau, 2007: Adjoint sensitivity of surface precipitation to initial conditions. *Mon. Wea. Rev.*, **135**, 2879-2896.

Marshall, J., and F. Molteni, 1993: Towards a dynamical understanding of planetary-wave flow regimes. *Q.J.R. Meteorol. Soc.*, **50**, 1792-1818.

Molteni, F., and T.N. Palmer, 1993: Predictability and finite-time instability of the northern winter circulation. *Q.J.R. Meteorol. Soc.*, **119**, 269-298.

Moore, A.M., H.G. Arango, A.J. Miller, B.D. Cornuelle, E. Di Lorenzo, and D.J. Neilson, 2004: A comprehensive ocean prediction and analysis system based on tangent linear and adjoint components of a regional ocean model. *Ocean Modell.*, **7**, 227-258.

Mu M., W. Duan, and B. Wang, 2003: Conditional nonlinear optimal perturbation and its applications. *Nonlinear Processes in Geophysics*, **10**, 493-501.

Oortwijn, J. and J. Barkmeijer, 1995: Perturbations that optimally trigger weather regimes. *J. Atmos. Sci.*, **52**, 3922-3944.

Opsteegh, J.D., R.J. Haarsma, F.M. Selten, and A. Kattenberg, 1998: ECBILT: a dynamic alternative to mixed boundary conditions in ocean models. *Tellus*, **50A**, 348-367

Palmer, T.N., R. Gelaro, J. Barkmeijer, and R. Buizza, 1998: Singular vectors, metrics and adaptive observations. *J. Atmos. Sci.*, **55**, 633-653.

Rabier, F., P. Courtier, and O. Talagrand, 1992: An application of adjoint models to sensitivity analysis. *Beitr. Phys. Atmos.*, **65**, 177-192.

Rabier, F., E. Klinker, P. Courtier, and A. Hollingsworth, 1996: Sensitivity of forecast errors to initial conditions. *Q.J.R. Meteorol. Soc.*, **122**, 121-150.

Reynolds, C.A., R. Gelaro, and T.E. Rosmond, 2006: A comparison of variance and total energy singular vectors. *Q.J.R. Meteorol. Soc.*, **131**, 1955-1973.

Schrier, Van der G., S.S. Drijfhout, W. Hazeleger, and L. Noulin, 2007: Increasing the Atlantic subtropical jet cools the circum-North Atlantic region. *Meteorol. Z.*, **16**, 1-10.

Sévellec, F., T. Huck, M. Ben Jelloul, N. Grima, J. Vialard, and A. Weaver, 2008: Optimal surface salinity perturbations of the meridional overturning and heat transport in a global ocean general circulation model. *J. Phys. Oceanogr.*, **38**, 2739-2754.

Tanguay, R.E., and S. Polavarapu, 1999: The adjoint semi-Lagrangian treatment of the passive tracer equation. *Mon. Wea. Rev.*, **127**, 551-564.

Zadra, A., M. Buehner, S. Laroche, and J.-F. Mahfouf, 2004: Impact of the GEM simplified physics on extratropical singular vectors. *Q.J.R. Meteorol. Soc.*, **130**, 2541-2569.